Acta Geodyn. Geomater., Vol. 16, No. 1 (193), 39–54, 2019
DOI: 10.13168/AGG.2019.0004
journal homepage: https://www.irsm.cas.cz/acta

ORIGINAL PAPER

TESTS ON THE DYNAMIC FAILURE RULES OF COAL-ROCK COMPOSITES

Zhongcheng QIN [1], Guangbo CHEN [1]*, Guohua ZHANG [2], Qinghai LI [1] and Tan LI [1]

[1] *College of Mining and Safety Engineering, Shandong University of Science and Technology, Qingdao, Shandong 266590, China*
[2] *School of Mining Engineering, Heilongjiang University of Science and Technology, Harbin, Heilongjiang 150022 , China*

**Corresponding author's e-mail:* cgb150617@126.com

ARTICLE INFO

Article history:
Received 29 August 2018
Accepted 14 January 2019
Available online 5 February 2019

Keywords:
Rock burst
Energy
Coal-rock composite
Dynamic failure
Experimental study

ABSTRACT

Coal measure strata are composed of multiple interbedding strata with different hardnesses. A sudden release of energy that was stored in surrounding rocks of tunnels may induce a rock burst; however, the specific strata in which the energy is accumulated cannot be accurately determined, thereby leading to ineffective prevention and management techniques for rock bursts. To address this problem, this study conducted axial loading tests on three different types of rock specimens (coal, gritstone and fine sandstone) and their composite specimens, and ascertained the energy accumulation rules of various components of the composites prior to a buckling failure. According to the results: for the coal-bearing binary composite specimens, the energy accumulated in coal occupied 88.5 %, 79.0 %, 71.4% and 79.6 % of the total energy accumulated in the specimens respectively; for the binary composite specimens composed of gritstone and fine sandstone, the energy accumulated in gritstone took up 61.2 % and 76.5 % of the total energy accumulated in the specimens respectively; and for the ternary composites, the energy accumulated in the coal occupied 79.8 %, 74.0 % and 76.3 % of the total energy accumulated in the specimens respectively, followed by the energy accumulated in the gritstone (12.1 %, 22.0 % and 18.8 %), and finally by the energy accumulated in the fine sandstone (only 8.1 %, 4.0 % and 4.9 %). Accordingly, in the composite rock strata, a small amount of energy was stored, and energy accumulation was more difficult in competent rock with large elastic moduli, while non-competent strata with small elastic moduli were preferable with regard to energy storage and accumulation. It can thus be concluded that the energy in coal-rock composites was accumulated mainly in non-competent strata, i.e., non-competent strata were key energy strata; additionally, the greater the difference in the hardness of the various components, the stronger the impact effect on the composite specimen.

1. INTRODUCTION

Coal is the most abundant form of fossil fuel out of all the geological resources in China. In terms of proven coal reserves, China now ranks third in the world and possesses 11.67 % of the world's total coal reserves (Mazaira and Konicek, 2015; Liu et al., 2009; Heriawan and Koike, 2008; Warwick et al., 2002). With the increasing depth and intensity of mining in China, an increasing amount of high-powered, long-haul-distance, highly reliable and fully-mechanized mining/caving equipment has been employed in underground mines, leading to constant and rapid advancements; however, various mine disasters, especially rock bursts, are occurring with increasing frequency and intensity (Fujii et al., 1997; Xie et al., 2012). Rock bursts are worldwide geological disasters, and almost all mines in the various coal producing countries of the world have suffered from this phenomenon. To date, researchers in China and elsewhere have conducted a great deal of research on the following aspects of rock bursts (Zhang et al., 2017; He et al., 2016): (1) the occurrence mechanism, (2) monitoring and forecasting, and (3) prevention and management. According to some long-term field application results, the prevention and control of a rock burst is difficult due to complex geological conditions and a variety of mining methods; this suggests that the management of this problem is currently sub optimal. Therefore, it is necessary to gain more knowledge about the occurrence mechanism of a rock burst in order to develop some optimal prevention and management techniques. Researchers from all over the world have established various theories regarding the occurrence mechanism of rock bursts from multiple perspectives; these include mainly strength theory, stiffness theory, energy theory, rock tendency theory, deformation instability theory and three-criterion theory (Dou et al., 2005; Xiong, 2014; Li et al., 2008). However, researchers are now paying an increasing amount of attention to energy theory. For an ore body/surrounding rock system, when the internal and external physical variations and the mechanical equilibrium state under stress reach the ultimate

Cite this article as: Qin Z, Chen G, Zhang G, Li Q, Li T: Tests on the dynamic failure rules of coal-rock composites. Acta Geodyn. Geomater., 15, No. 1 (193), 39–54, 2019. DOI: 10.13168/AGG.2019.0004

failure conditions, the accumulated elastic energy in the system exceeds the energy consumed for the system failure, and the excessive elastic energy is dissipated towards the outside world. This can result in an impact on the fractured coal-rocks and trigger the occurrence of a rock burst (Chen et al., 2009). To date, the investigations of rock bursts from the perspective of energy have only been conducted via laboratory tests, theoretical calculations and mathematical modeling. An in-depth investigation based on energy theory includes the following procedures. Firstly, according to the research results of a rock failure's energy mechanism, a rock failure is closely related to energy dissipation; specifically, damage to coal-rocks can be triggered by the dissipation of energy, while different failure modes correspond to different energy dissipation modes. Next, the energy variation of surrounding rocks is examined by taking them as a whole. When the dissipated strain from the surrounding rocks exceeds the energy consumed by the ore body, a rock burst may be induced. Then, the accumulation region of the surrounding rock energy under the effects of the excavation process in a mining tunnel and a roof fracture can be ascertained through numerical simulations. When using energy theory, the surrounding rock system is treated as a whole. In fact, the coal measure strata are composed mainly of competent and non-competent rocks (Stachy, 2016), thus exhibiting unique lithological combination characteristics. The related engineering properties depend to a great degree on the thicknesses of competent and non-competent rocks and the combination modes (Tang et.al., 2017; Liu et al., 2015; Ikari et al., 2015). Since coal measure strata differ in hardness, they exhibit different energy accumulation behaviors (Liu et al., 2016; Zhang and Feng, 2015; Zhou et al., 2017). Through the use of energy theory, the failure criterion of coal-rocks has been proposed, and as a result the rock burst tendency can be predicted; however, the specific positions of energy accumulation in coal-rocks have still not been investigated adequately and the related energy accumulation rules are still unknown. The determination of a specific stratum remains the key to preventing rock bursts.

In recent years, a great deal of research, which has focused on coal-rock combination bodies, has been conducted, and some significant results have been obtained and reported. For example, the research conducted by Qi et al. and Liu et al. (Qi and Dou, 2008; Liu et al., 2004) on different coal-rock combination bodies and the rock burst mechanism, ascertained that employing a coal-rock combination body to determine the tendency of a rock burst was more in accordance with the actual underground conditions. Dou et al., along with other authors (Dou et al., 2005; Lu et al., 2007; Zhao et al., 2008), studied the rock burst tendency and precursor information of the acoustoelectric effect, and their tests proved that coal-rock combination bodies could suddenly lose their instability. Zuo et al. (Zuo et al., 2013) found that the failure of a combined coal-rock mass mainly occurred inside the coal, and the confining pressure, combination modes, and loading conditions played a very important role on the failure mode of the combined samples. Petukhov and Linkov (Petukhov and Linkov, 1979) analyzed the stability of the general bipartite system and roof-coal system when studying the stable behavior of a rock mass after the postpeak point. Vakili and Hebblewhite (Vakili and Hebblewhite, 2010) developed a new cavability assessment criterion for top-coal embedded in a combined coal-rock system, composed of an immediate roof, top coal, cutting coal, and floor, by numerical modeling. Mohtarami et al. (Mohtarami et al., 2014) studied the interaction between soil mass and downward rock blocks as a combined structure by using a theoretical model for stability analysis. Unfortunately, there is less research on the location of energy accumulation in coal-rock composites. Therefore, the energy accumulation law cannot be assessed, and the accumulation position of the energy that triggers a rock burst in a coal- rock system cannot be analyzed.

To overcome the above problems, this study conducted uniaxial compressive tests on coal, gritstone and fine sandstone specimens in order to investigate the pre-peak energy accumulation behaviors. Next, these three types of specimens were combined in pairs or together, and the models of binary and ternary composites were established. Uniaxial compressive failure tests were then conducted on these binary and ternary composite specimens in order to investigate the energy storage of each component and ascertain the related energy accumulation rules. This study could provide a theoretical underpinning for determining the energy accumulation position in a vertical direction, and thus lead to a more targeted prevention and management technique for rock bursts.

2. BASIC DEFORMATION AND FRACTURE TESTS ON COAL-ROCKS

2.1. THE PREPARATION OF COAL-ROCK SAMPLES

During the past few years, rock bursts have occurred frequently in the Junde Coal Mine, Heilongjiang Province, China. Specimens from this mine were therefore selected in this study for an in-depth analysis. Before collecting the specimens, the geological conditions of the 17th coal seam, roof and floor in the Junde Coal Mine, and the sampling feasibility were first analyzed, and the regional representativeness of the specimens and discreteness of the related data were taken into account. Large coal bodies were first avalanched by blasting, and the collected specimens were wrapped in preservative films for sealing. Meanwhile, for each specimen, the sampling position and time were recorded. Finally, the collected specimens were placed in a wooden box and carried back to the laboratory for subsequent tests. According to the requirements as mandated by

Fig. 1 A picture of some prepared rock specimens.

(a) the testing machine (b) the extensometer

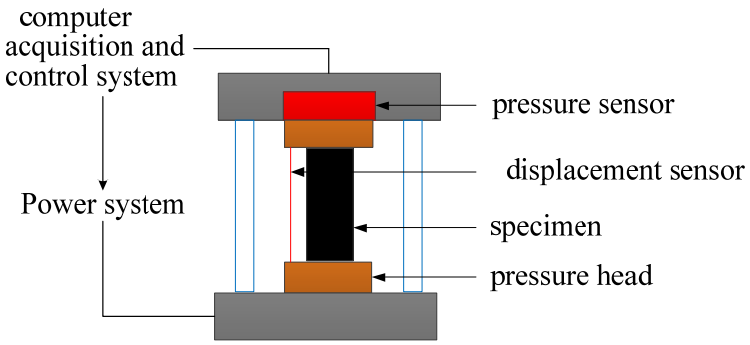

(c) a schematic diagram of the test system

Fig. 2 A picture of the rock testing system.

Chinese standards (Qi and Dou, 2008; Liu et al., 2004; Dou et al., 2005; Lu et al., 2007): the coal, gritstone and fine sandstone specimens with an identical diameter of 50 mm (φ=50 mm), denoted as C, G, and F, were first prepared using an automatic core drilling machine; next, the specimens were cut by a cutting machine, and specimens with an identical height of 100 mm (h=100 mm) were prepared; finally, using a dual-face grinding machine, the specimens were polished until the unevenness degrees of the two end surfaces were smaller than 0.05 mm. The other indexes of coal specimens were measured in accordance with the international physical and mechanical measurement methods of coal and rocks. For reducing data discreteness, all specimens were cut from the same rock, and 18 standard coal, gritstone and fine sandstone specimens in total, denoted as C1~C6, G1~G6 and F1~F6, were prepared. Figure 1 shows a picture of some of the specimens.

2.2. THE EXPERIMENTAL SYSTEM AND METHOD

The tests in this study were conducted using the microprocessor-controlled electro-hydraulic servo rock-shear rheological test system (TYJ-500KN). Figures 2(a) and 2(b) display pictures of the testing machine and the extensometer that were used in this study, while Figure 2(c) illustrates the structure of the test system. The control valve was imported from Germany, and ensures the control precision in the load/unloading process. During the entire test process, the load was controlled precisely by a computer, data were acquired automatically in real time and the high-

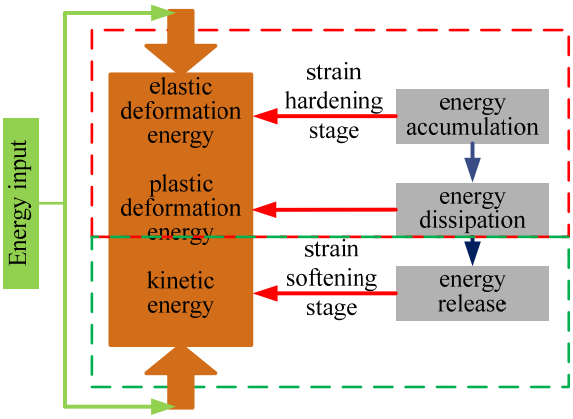

Fig. 3 An illustration of the energy transformation process in the coal-rock under the loading process.

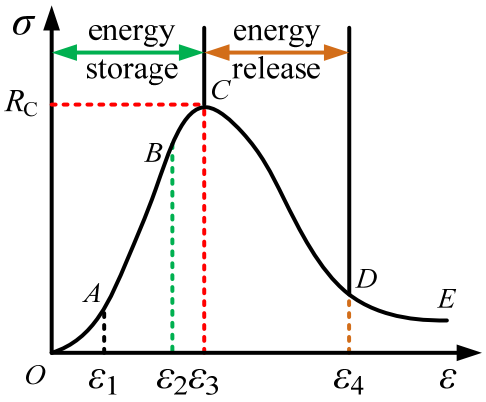

Fig. 4 A typical complete stress-strain curve of a rock specimen under uniaxial compression and deformation.

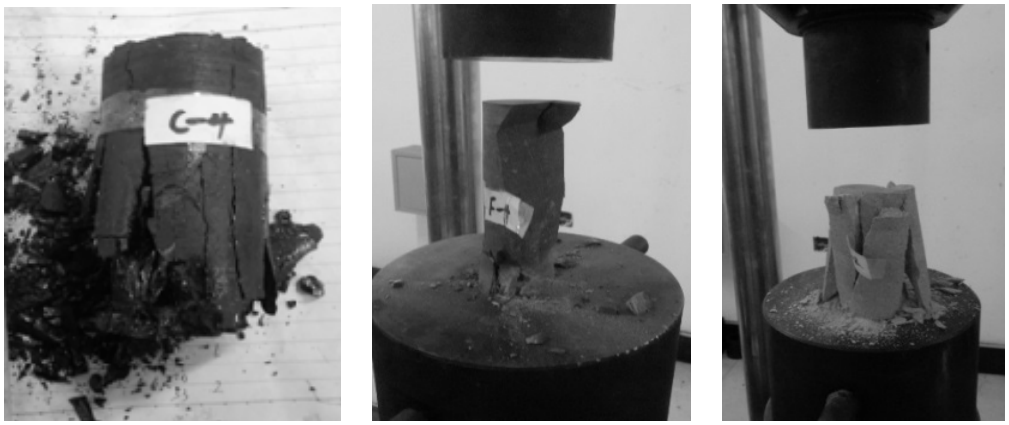

(a) Coal (b) Fine sandstone (c) Gritstone

Fig. 5 The failure forms of different types of specimens.

precision stress-strain curves of the coal specimens were plotted and outputted. The sampling frequency, the accuracy of the axial displacement sensor and the accuracy of the load sensor were set as 50 Hz, 0.00001 mm and 0.001 kN respectively.

During the load process, the energy transformation was driven mainly by the strain hardening and softening, which can be divided into four stages; namely, the energy input stage (i.e., energy was provided by the press machine), energy accumulation stage (i.e., the accumulation of elastic energy), energy dissipation stage (i.e., the dissipation of plastic energy) and energy release stage (i.e., the release of kinetic energy and radiant energy amongst others). Figure 3 displays the entire energy transformation process when a load was applied to rock specimens.

For the acquired complete stress-strain curves (O→A→B→C→D→E (see Fig. 4)), a deformation control was adopted in the tests in this study (Zhao et al., 2008), during which the strain was applied at a rate of 0.005 mm/s until the specimen was finally fractured. Specifically, in a complete stress-strain curve, OA represents the compaction phase, AB represents the linearly elastic phase, BC represents the plastic yield phase and CD represents the the failure phase.

2.3. AN ANALYSIS OF THE EXPERIMENTAL RESULTS

Uniaxial compressive tests were carried out on different coal, fine sandstone and gritstone specimens at a loading rate of 0.005 mm/s, during which the loading process was controlled by the displacement. Figure 5 shows the failure forms of certain specimens, Table 1 lists the mean values of various parameters, and Figure 6 displays some representative stress-strain curves of different specimens.

The following conclusions can be drawn from Figure 5. Under a uniaxial compression, the coal specimen was crushed, and many fractures and cracks were distributed nonuniformly in the specimen and grew rapidly; furthermore, the coal specimen was almost crushed completely, suggesting a plastic

Table 1 The experimental results and data processing.

Specimen type	Serial number	R_c/MPa		E/MPa		E_s/kJ/m^3		E_x/kJ/m^3		K_E		Judgment standard	Rock burst tendency
		Discrete value	Mean value	Discrete value	Mean value	Discrete value	Mean value	Discrete value	Mean value	Discrete value	Mean value		
C	C-1	11.35	11.56	976.71	957.61	0.106	0.099	0.022	0.017	5.494	7.615	$K_E \geqslant 5.0$	Strong
	C-2	13.70		958.83		0.098		0.027		3.614			
	C-3	9.92		936.84		0.083		0.009		12.872			
	C-4	11.15		940.24		0.102		0.018		5.671			
	C-5	12.36		957.62		0.113		0.013		8.692			
	C-6	10.89		972.41		0.094		0.01		9.401			
F	F-1	130.34	126.18	4344.67	3677.56	21.032	18.213	9.568	7.782	2.615	2.436	$5.0 \leqslant K_E < 1.5$	Weak
	F-2	124.56		3161.42		13.259		6.236		2.190			
	F-3	127.27		3928.09		16.949		8.206		2.068			
	F-4	125.52		3521.73		18.449		8.339		2.212			
	F-5	129.18		3629.87		19.281		7.381		2.612			
	F-6	120.83		3479.59		20.309		6.962		2.917			
G	G-1	50.48	54.35	2567.23	2437.58	3.206	2.627	0.985	0.927	3.234	2.865	$5.0 \leqslant K_E < 1.5$	Weak
	G-2	52.98		2280.25		2.965		1.235		2.363			
	G-3	58.36		2570.72		2.100		0.744		2.986			
	G-4	55.28		2274.18		2.428		0.881		2.755			
	G-5	57.31		2431.63		2.179		0.804		2.710			
	G-6	51.69		2501.46		2.886		0.917		3.146			

Note: C—Coal; F—Fine sandstone; G—Gritstone; R_c—Compressive strength; E—Elastic modulus; E_s—Pre-peak energy; E_x—Post-peak energy; K_E—Energy index of rock-burst (these apply throughout the paper)

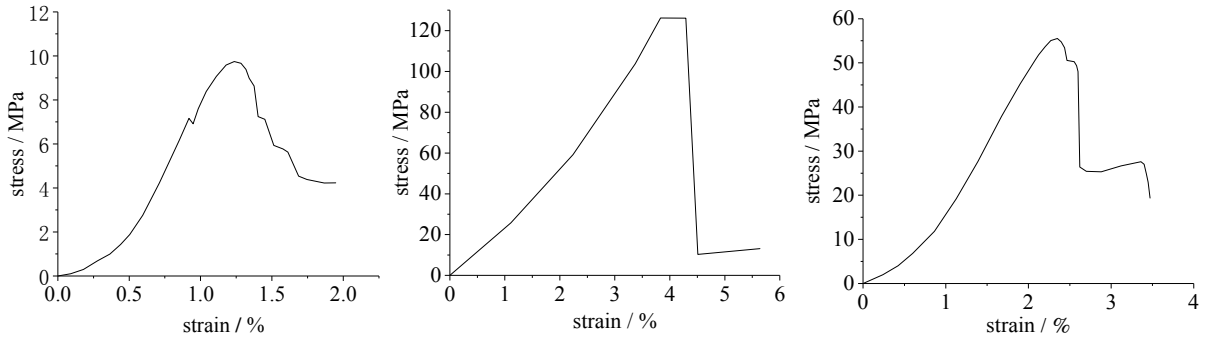

(a) Coal (b) Fine sandstone (c) Gritstone

Fig. 6 Some representative stress-strain curves of different types of specimens.

failure. The gritstone exhibited a columnar splitting failure and was evenly fractured, with cracks developing vertically; i.e., the gritstone underwent a semi-plastic failure. Prior to the failure, the fine sandstone showed no obvious signs, but made a loud noise at the point of failure; moreover, in the fine sandstone specimen, a nonuniform and brittle failure occurred.

Figure 6 shows the complete stress-strain curves of different specimens during the compression process. In the compaction phase: because of the constant closing of fractures and pores in the coal, a long compaction process can be easily observed, during which the stress and deformation were both large; the gritstone specimen was more uniform than the coal specimen and exhibited a short compaction

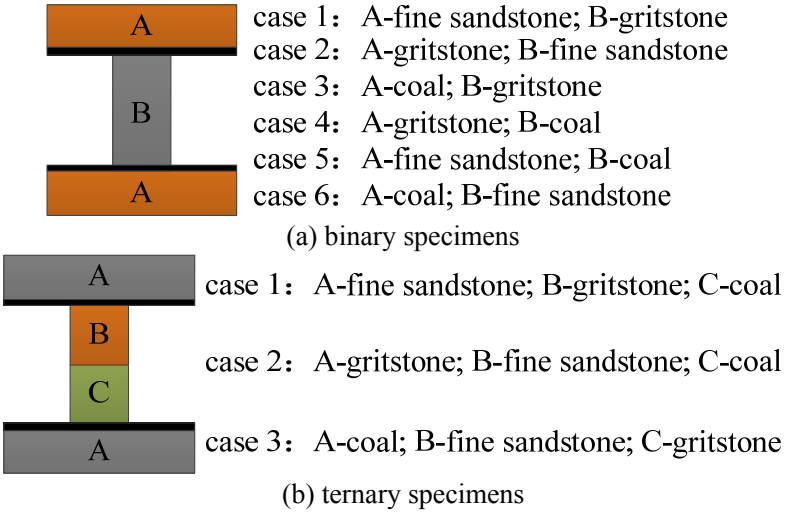

Fig. 7 The combination modes of the different composite specimens.

process, during which the stress was large but the deformation was slight; and by contrast, the fine sandstone specimen showed no obvious compaction process. In the linearly-elastic phase: since weak fractures in the coal developed gradually and were interconnected, the coal specimen then underwent a short and unstable linearly-elastic phase; and due to the highest heterogeneity and largest elastic modulus, the fine sandstone specimen underwent the longest linearly elastic phase. In the plastic phase: new cracks were formed in the coal and the original cracks were interconnected, leading to an overall unstability, and therefore, the coal's plastic phase was long; and the fine sandstone specimen was destroyed abruptly and no obvious plastic phase was observed. In the final failure phase: on account of the rapid development of cracks, the fine sandstone specimen was destroyed abruptly and completely in a short space of time, and the related stress-strain curve was a straight line; on the other hand, after multiple, gradual failures, the coal and gritstone specimens were not destroyed completely for a long period of time.

As listed in Table 1: the fine sandstone specimen had the greatest uniaxial compressive strength, which was 10.9 times and 2.3 times larger than the values of the coal and gritstone specimens respectively; and the pre-peak accumulated energy of the fine sandstone was also the greatest, being 183.97 times and 6.93 times larger than the values of the coal and gritstone specimens respectively. Under the same stress conditions, the least energy was accumulated in the fine sandstone specimen while the most energy was accumulated in the coal specimen. The impact energy index of the coal was 7.615; i.e., the rock burst tendency of the coal is strong, whilst that of the gritstone and fine sandstone is moderate.

3. TESTS ON THE COMPOSITE COAL-ROCK SPECIMENS

3.1. THE PREPARATION OF THE COMPOSITE SPECIMENS

In the field engineering domain, the coal seam, roof and floor constitute a balanced system; furthermore, under a large crustal stress, a large amount of energy is accumulated in the system, and a rock burst will be triggered when the accumulated energy is released suddenly (Zuo et al., 2013; Petukhov and Linkov, 1979). For investigating the energy storage capacities of the various components of the composite specimens prior to failure, some binary and ternary composite specimens were prepared, as shown in Figure 7. The test results of these composite specimens can help ascertain the energy accumulation rules of the composites prior to failure.

The combination of specimens should obey the following rules:

1. The upper and lower rocks should be from the same type of strata and show no difference in lithology; and the middle rock should be a standard specimen (φ=50 mm, h=100 mm);
2. During the tests, the middle standard specimen should first be fractured, and the related parameters should satisfy the requirement: $S_{\text{upper/lower}} > R_{\text{c\_middle}} / R_{\text{c\_upper/lower}} \cdot S_{\text{middle}}$ (where S_{upper}, S_{lower} and S_{middle} denote the sectional areas of the upper, lower and middle rocks respectively, and $R_{\text{c\_middle}}$, $R_{\text{c\_upper}}$ and $R_{\text{c\_lower}}$ denote the compressive strengths of the middle, upper and lower rocks respectively).
3. When the contact areas of the upper and lower rocks are different, steel plates with a strong degree of stiffness and slight deformation were arranged between the upper/lower and middle rocks.

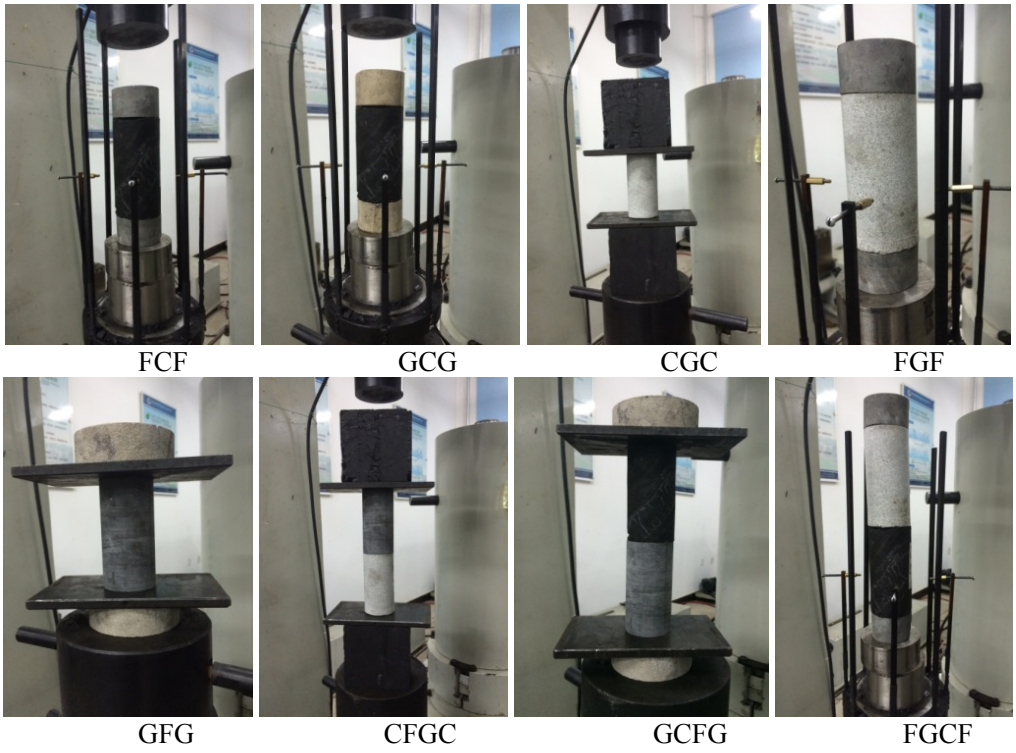

Fig. 8 Pictures of certain composite specimens.

4. The angle between the coal and rock specimens is 0 °, and the components are in direct contact with each other in order to maintain the original superimposed interbedded state in engineering as much as possible. If an adhesive is used in the combination process, the inherent properties, amount and bonding action of the adhesive will all have a significant influence on the properties of the combination.

Six different binary specimens (i.e., two-component specimens) were prepared; specifically, the coal and gritstone constituted 2 composite specimens, denoted as GCG and CGC, the coal and fine sandstone constituted 2 composite specimens, denoted as CFC and FCF, and the gritstone and fine sandstone constituted 2 composite specimens, denoted as GFG and FGF. Additionally, 3 different ternary specimens consisting of three components were prepared, denoted as FGCF, GFCG and CGFC. The pictures of certain specimens are presented in Figure 8. For each composite specimen, 6 groups of tests were conducted for averaging purposes.

3.2. AN ANALYSIS OF TEST RESULTS, DEFORMATION CURVES AND THE FAILURE MODE

During the tests, a load was applied on the composite specimens at a rate of 0.005 mm/s in a displacement-controlled mode. For each specimen, the stress-strain curve, various parameters and failure form were investigated, with the results shown in Figure 9 (In the process of the experiment, the axial displacement of the composite specimen is measured automatically by the testing machine, and the strain of the composite specimen can be obtained by computer processing system.), Table 2 and Figure 10 respectively.

3.3. AN ANALYSIS OF THE TEST RESULTS

For reducing any test errors, the measured values of various parameters were averaged (see Table 3). It can be observed that the composite specimens were comparable to the damaged component with regard to compressive strength; and both the upper and lower rocks were not destroyed, and can be regarded as undamaged cushion layers.

With regard to the pre-peak energy (E_s), little energy was accumulated in the coal standard specimen. For the composite specimens, a lot of energy was accumulated in the coal prior to failure; and the smaller the compressive strength of the combined specimen, the smaller the accumulated energy of the combined specimen. Accordingly, before a rock burst occurs, more energy is accumulated in non-competent rocks than in competent rocks.

In terms of the impact energy index (K_E), the composite specimens of coal and fine sandstone were the greatest, followed by the composite specimens of coal and gritstone, while the composite specimens of gritstone and fine sandstone were lowest. It can thus be concluded that the larger the difference in hardness between the various components in the specimen, the greater the impact energy index. For the specimens in

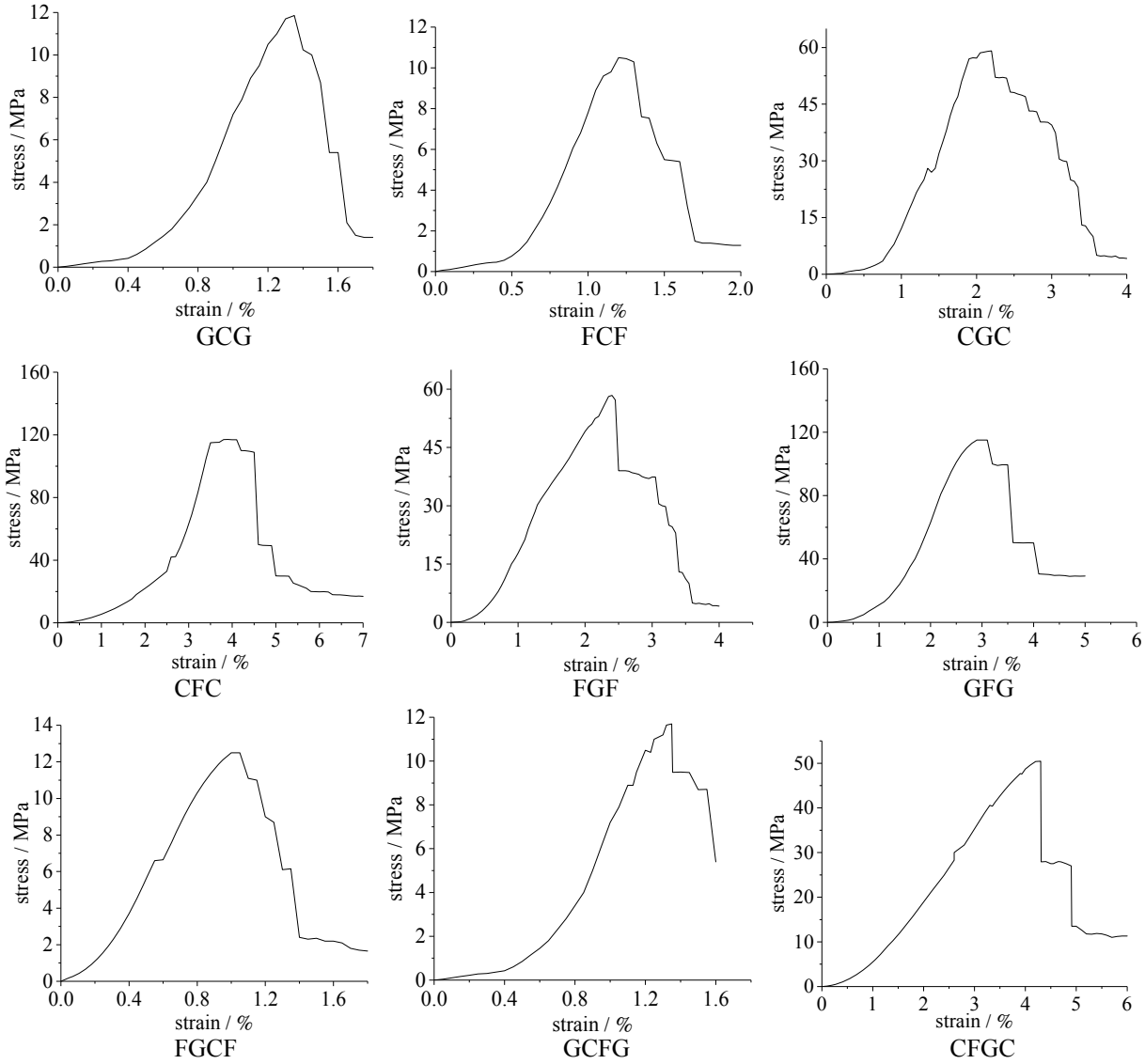

Fig. 9 The representative stress-strain curves of certain composite specimens.

which the components vary more significantly with regard to hardness, the impact energy index was larger and the rock burst tendency was stronger.

As shown in Figure 15, the coal in the composite specimens was crushed completely into a large number of fragments, the gritstone underwent an incomplete failure and was broken into a few large fragments, while the fewest large fragments were caused by the failure of the fine sandstone. Accordingly, the coal was poor with regard to compressive strength, and underwent a plastic failure under compression; the gritstone exhibited a columnar failure, which can be regarded as a semi-plastic failure; and the sandstone displayed some obvious brittle failure characteristics.

4. A DETERMINATION OF KEY ENERGY STRATA

4.1. THE CALCULATION OF THE ACCUMULATED ENERGY IN EACH COMPONENT OF THE COMPOSITE SPECIMENS

The forces impacting upon the composite specimens were then analyzed. As shown in Figure 11(a), the action and reaction are equal and opposite (Vakili and Hebblewhite, 2010); therefore,

$$F_1=F_2 \tag{1}$$

$$\sigma_1 \times S_1=\sigma_2 \times S_2 \tag{2}$$

For a composite specimen, given the compressive strength (σ_2), the stress on the middle specimen (σ_1) can be calculated as:

$$\sigma_1=(\sigma_2 \times S_2) / S_1 \tag{3}$$

Table 2 Some test data of the composite specimens.

Composite specimen	Serial number	R_c/MPa	E/MPa	E_s/(kJ/m^3)	E_x/(kJ/m^3)	K_E
GCG	GCG-1	18.98	1543.98	0.125	0.022	5.682
	GCG-2	8.95	1361.05	0.119	0.024	4.958
	GCG-3	9.69	1220.34	0.128	0.025	5.120
	GCG-4	8.50	1567.35	0.123	0.025	4.920
	GCG-5	11.86	1278.02	0.126	0.024	5.250
	GCG-6	8.70	1324.05	0.132	0.027	4.889
FCF	FCF-1	10.53	1049.28	0.102	0.017	6.005
	FCF-2	9.98	1185.61	0.103	0.013	7.923
	FCF-3	10.49	1088.54	0.112	0.019	5.895
	FCF-4	18.69	1083.88	0.106	0.018	5.889
	FCF-5	9.48	995.73	0.107	0.020	5.350
	FCF-6	8.97	1105.48	0.096	0.019	5.053
CGC	CGC-1	50.46	1528.53	12.820	3.305	3.879
	CGC-2	61.98	1603.48	13.822	3.451	4.055
	CGC-3	53.88	1588.91	12.915	3.690	3.500
	CGC-4	50.84	1479.38	12.934	2.627	4.924
	CGC-5	50.63	1602.02	12.839	2.666	4.816
	CGC-6	59.02	1328.82	11.932	2.526	4.723
CFC	CFC-1	113.47	1029.27	87.312	10.647	8.201
	CFC-2	145.02	1285.62	80.634	10.313	7.819
	CFC-3	120.88	1078.53	79.091	10.615	7.451
	CFC-4	134.32	1093.48	86.234	8.759	9.845
	CFC-5	129.09	995.53	94.455	11.058	8.542
	CFC-6	126.11	1108.32	92.912	10.438	8.901
FGF	FGF-1	50.30	2489.21	3.521	1.371	2.568
	FGF-2	60.98	2379.38	3.602	1.901	1.894
	FGF-3	49.80	2505.29	3.632	1.722	2.109
	FGF-4	55.35	2498.18	2.771	1.271	2.180
	FGF-5	54.88	2638.38	2.660	1.312	2.027
	FGF-6	50.09	2702.31	2.690	1.035	2.511
GFG	GFG-1	107.45	2861.65	67.312	21.028	3.201
	GFG-2	127.08	2869.18	64.634	22.513	2.871
	GFG-3	141.22	2689.94	72.016	26.742	2.693
	GFG-4	109.76	2748.26	69.338	22.861	3.033
	GFG-5	121.89	2931.83	70.809	27.297	2.594
	GFG-6	131.03	3038.79	65.841	22.838	2.883
FGCF	FGCF-1	8.39	1839.31	0.092	0.015	6.218
	FGCF-2	9.98	2021.54	0.108	0.018	5.881
	FGCF-3	16.24	1788.34	0.090	0.013	7.005
	FGCF-4	8.78	1982.65	0.106	0.020	5.429
	FGCF-5	10.40	2286.49	0.090	0.012	7.233
	FGCF-6	11.19	2501.36	0.108	0.016	6.918
GCFG	GCFG-1	9.54	2781.81	0.132	0.021	6.286
	GCFG-2	9.57	2893.98	0.110	0.018	6.002
	GCFG-3	17.09	2909.48	0.124	0.022	5.636
	GCFG-4	10.78	2971.83	0.122	0.015	8.402
	GCFG-5	11.88	3008.49	0.130	0.013	9.776
	GCFG-6	9.75	2598.68	0.144	0.023	6.182
CFGC	CFGC-1	61.44	2389.67	10.892	1.588	6.859
	CFGC-2	56.89	2945.58	15.502	1.981	7.825
	CFGC-3	47.79	3127.64	12.326	1.700	7.250
	CFGC-4	45.59	2961.48	17.002	2.602	6.534
	CFGC-5	62.28	2783.35	15.568	2.677	5.815
	CFGC-6	55.71	2865.39	12.392	1.842	6.729

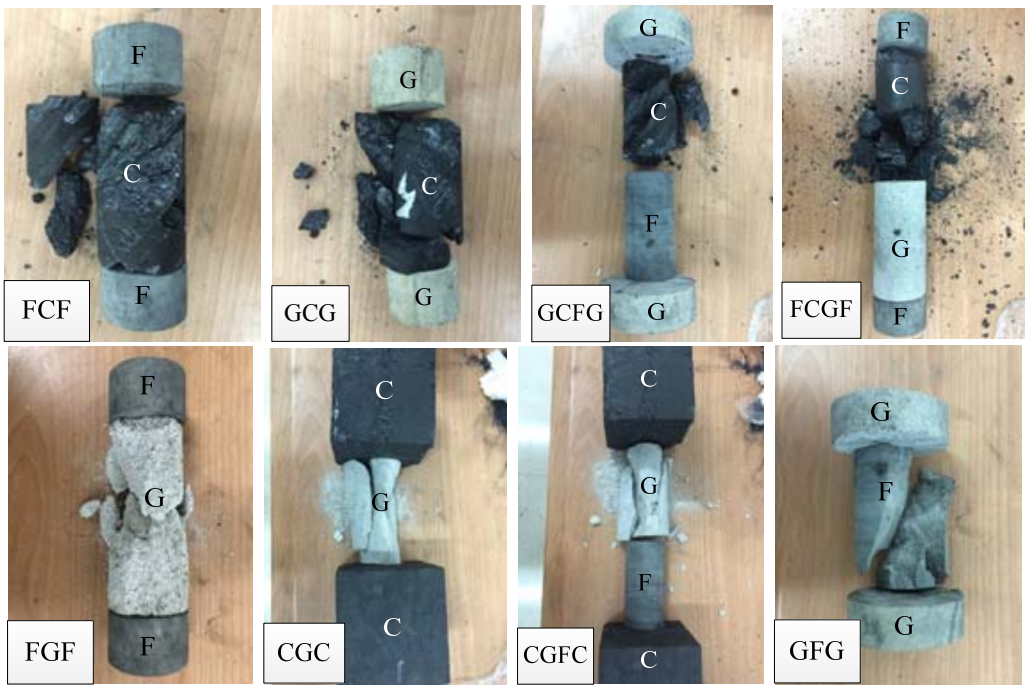

Fig. 10 The failure forms of certain composite specimens.

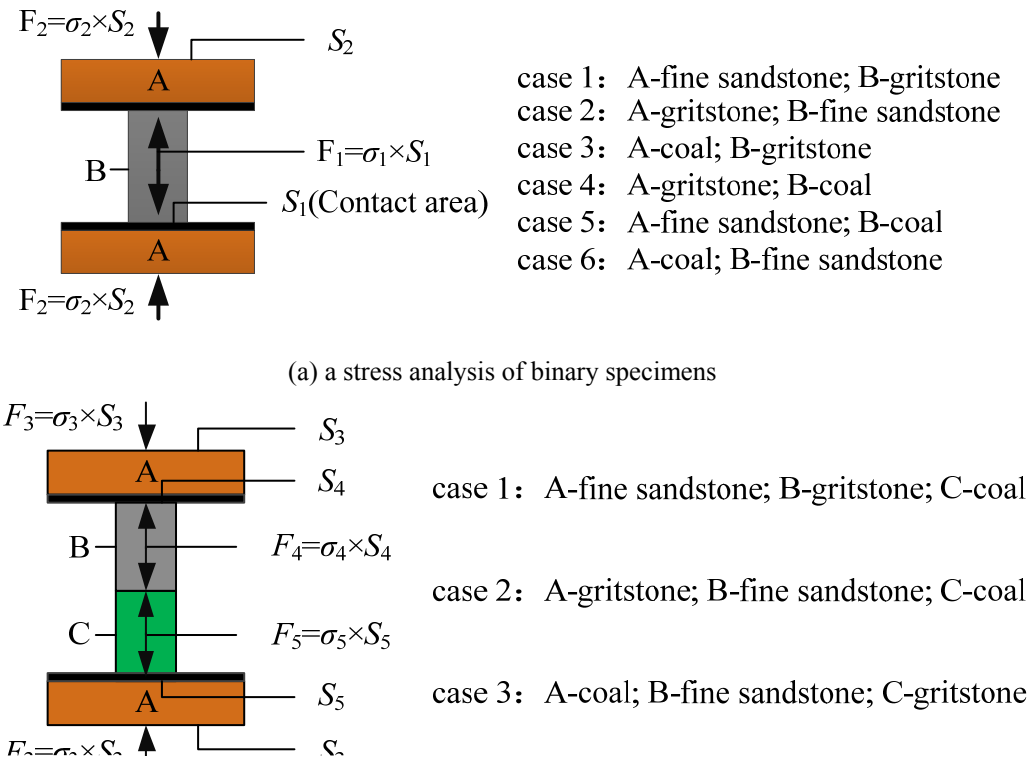

Fig. 11 An analysis of the forces applied on the composite specimen.

Table 3 The average test data of the composite specimens.

Composite specimen	R_c/MPa	E/MPa	E_s/(kJ/m^3)	E_x/(kJ/m^3)	K_E	Identification standard	Rock burst tendency
GCG	11.11	1382.47	0.126	0.0245	5.137	$K_E \geq 5.0$	Strong
FCF	11.36	1084.76	0.104	0.018	6.019	$K_E \geq 5.0$	Strong
CGC	54.47	1521.86	12.877	3.044	4.316	$5.0 \leq K_E < 1.5$	Weak
CFC	128.15	1098.46	86.773	10.305	8.460	$K_E \geq 5.0$	Strong
FGF	53.57	2535.46	3.146	1.435	2.215	$5.0 \leq K_E < 1.5$	Weak
GFG	123.07	2856.61	68.325	23.880	2.879	$5.0 \leq K_E < 1.5$	Weak
FGCF	10.83	2069.95	0.099	0.016	6.447	$K_E \geq 5.0$	Strong
GCFG	11.27	2860.71	0.127	0.019	7.047	$K_E \geq 5.0$	Strong
CFGC	54.95	2845.52	13.947	2.065	6.835	$K_E \geq 5.0$	Strong

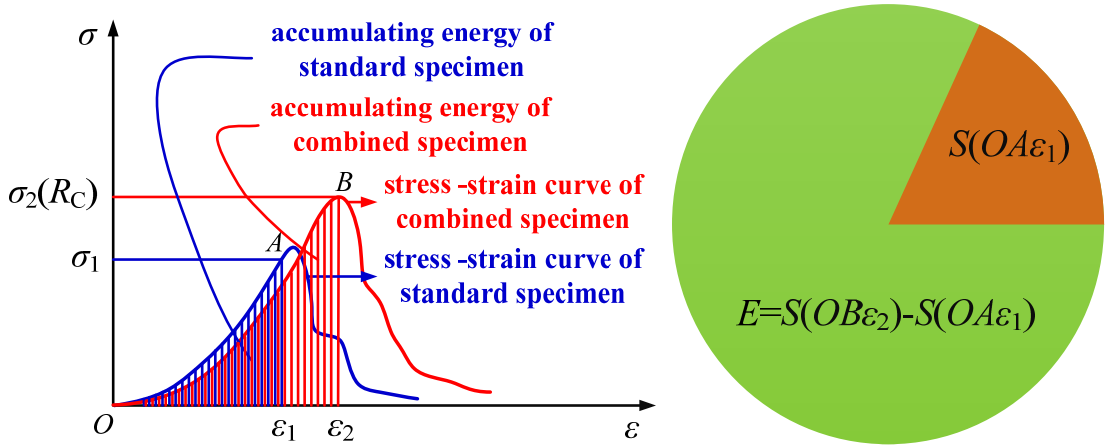

(a) an analysis of the energy distribution of the binary combination

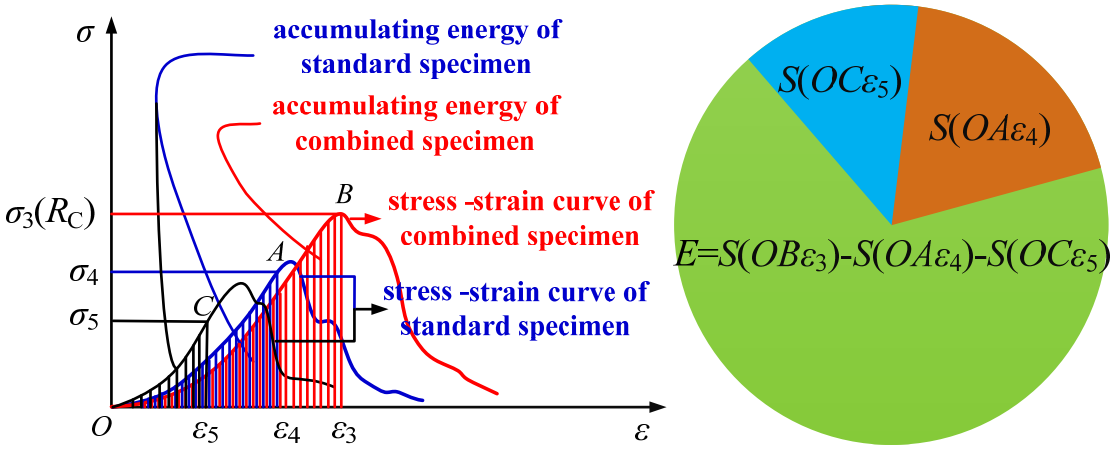

(b) an analysis of the energy distribution of the ternary combination

Fig. 12 An illustration of the calculation of the accumulated energy in different components.

Table 4 An analysis of the accumulated energy in different components of different composite specimens.

Composite specimen	Peak stress on the composite specimen / MPa	Total energy accumulated in the composite prior to failure / (kJ/m^3)	Damaged rock	Energy accumulated in the damaged rocks under peak stress / (kJ/m^3)	Energy accumulated in other rocks / (kJ/m^3)	Energy accumulation rock
GCG	11.11	0.126	C	C：0.090	G：0.036	C
FCF	11.36	0.104	C	C：0.092	F：0.012	C
CGC	54.47	12.877	G	G：2.627	C：10.250	C
CFC	128.15	86.773	F	F：18.213	C：68.560	C
FGF	53.57	3.146	G	G：1.926	F：1.220	G
GFG	123.07	68.325	F	F：16.075	G：52.250	G
FGCF	10.83	0.099	C	C：0.079	G：0.012 F：0.008	C
GCFG	11.27	0.127	C	C：0.094	G：0.028 F：0.005	C
CFGC	54.95	13.947	G	G：2.627	F：0.680 C：10.640	C

Figure 12(a) illustrates the calculation methods of the accumulated energy in different components. Using Origin (a data processing software), the energy accumulated in the middle specimen under the action of σ_1 was calculated and denoted as $S(OA\varepsilon_1)$. Subsequently, the energy accumulated in the upper and lower specimens (E) can be calculated as:

$$E= S(OB\varepsilon_2) - S(OA\varepsilon_1) \quad (4)$$

where $S(OB\varepsilon_2)$ denotes the total accumulated energy in the composite specimen.

In a similar way, for a ternary specimen, as shown in Figure 11(b) , the forces between the objects are:

$$F_3=F_4=F_5 \quad (5)$$

$$\sigma_3 \times S_3=\sigma_4 \times S_4=\sigma_5 \times S_5 \quad (6)$$

For a composite specimen, given the compressive strength (σ_3), the stress on the middle specimen (σ_4 and σ_5) can be calculated as:

$$\sigma_4=(\sigma_3 \times S_3) / S_4 \quad (7)$$
$$\sigma_5=(\sigma_3 \times S_3) / S_5 \quad (8)$$

Figure 12(b) illustrates the calculation methods of the accumulated energy in different components. Again using Origin, the energy accumulated in the middle specimen under the action of σ_4 was calculated and denoted as $S(OA\varepsilon_4)$; and the energy accumulated in the middle specimen under the action of σ_5 was calculated and denoted as $S(OC\varepsilon_5)$. Subsequently, the energy accumulated in the upper and lower specimens (E) can be calculated as:

$$E= S(OB\varepsilon_3)-S(OA\varepsilon_4)-S(OC\varepsilon_5) \quad (9)$$

where $S(OB\varepsilon_3)$ denotes the total accumulated energy in the composite specimen.

Table 4 lists the related calculation results of the accumulated energy in different components of the composite specimens.

4.2. AN ANALYSIS OF THE ENERGY CALCULATION RESULTS

The following conclusions can be drawn from Table 4.

1. For the composite GCG, the energy accumulated in the coal and gritstone occupied 71.4 % and 28.6 % of total energy accumulated in the specimen respectively; for the composite FCF, the energy accumulated in the coal and fine sandstone occupied 88.5 % and 11.5 % of total energy accumulated in the specimen respectively; for the composite CGC, the energy accumulated in the coal and gritstone occupied 79.6 % and 20.4 % of the total energy accumulated in the specimen respectively; for the composite CFC, the energy accumulated in the coal and fine sandstone occupied 79.0 % and 21.0 % of the total energy accumulated in the specimen respectively; for the composite FGF, the energy accumulated in the gritstone and fine sandstone occupied 61.2 % and 38.8 % of the total energy accumulated in the specimen respectively; and for the composite GFG, the energy accumulated in the gritstone and fine sandstone occupied 76.5 % and 23.5 % of the total energy accumulated in the specimen respectively.

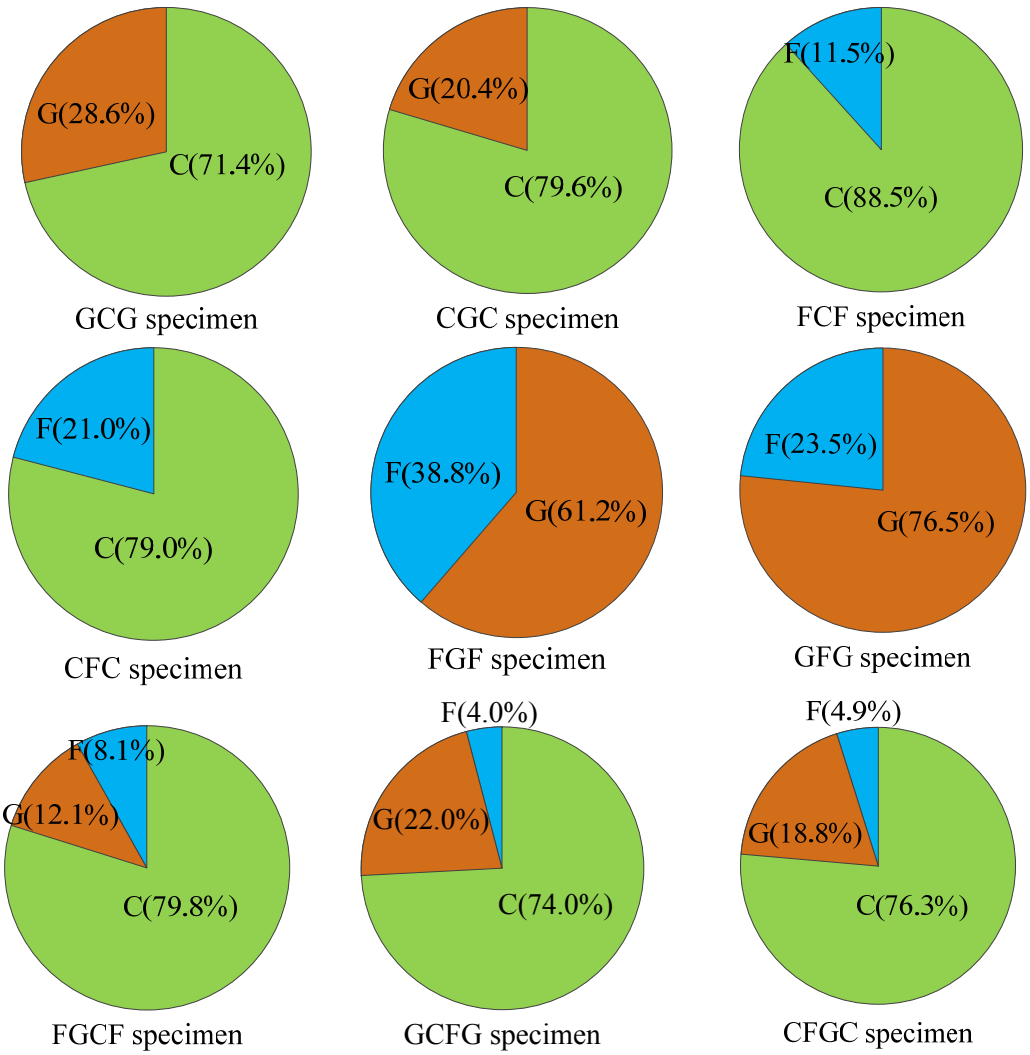

Fig. 13 Pie diagrams of the energy accumulations in different components of the composite .specimens

2. For the composite FGCF, the energy accumulated in the coal, gritstone and fine sandstone took up 79.8 %, 12.1 % and 8.1 % of the total energy accumulated in the specimen respectively; for the composite GCFG, the energy accumulated in the coal, gritstone and fine sandstone took up 74.0 %, 22.0 % and 4.0 % of the total energy accumulated in the specimen respectively; and for the composite CFGC, the energy accumulated in the coal, gritstone and fine sandstone took up 76.3 %, 18.8 % and 4.9 % of the total energy accumulated in the specimen respectively.

For a more visual display, in Figure 13 the proportions of energy accumulation in different components are presented in pie diagrams. Specifically, the energy accumulated in the coal, gritstone and fine sandstone are marked in green, yellow and blue respectively.

The overlying strata of the stope face, in which a lot of energy is accumulated, are referred to as key energy strata; furthermore, these strata dominate rock movements completely or locally. As shown in Figure 13, for the coal-bearing binary composite specimens, the energy was accumulated in coal; for the binary composite specimens, which did not include coal, the energy was accumulated in gritstone; and for the ternary composite specimens, most of the energy was accumulated in coal, followed by the energy accumulation in gritstone, and with the least energy being accumulated in fine sandstone. It can thus be concluded that in the composite coal strata consisting of different components with different hardnesses, the competent strata with great elastic moduli were barely deformed but exhibited a low energy storage, and it was difficult for them to accumulate energy; while it was more straightforward for the non-competent strata with a small elastic moduli to store and accumulate energy. Accordingly, the non-competent strata are key energy strata and play dominant roles in the occurrence of an overall rock burst.

5. DISCUSSION

In previous studies, some Chinese scholars also investigated in-depth the failure forms of composites. However, the composite specimens in their work and those in the present study differ in combination mode and type. For example, Qi Qingxin et al. focused on the inclination angle, confining pressure, loading condition and combination ratios of the composite specimens; and although they examined the energy in the specimens, the energy accumulations in different components were poorly investigated. It is well-known that a rock burst can be triggered under certain energy conditions, and a sudden energy release is the main reason for a rock burst occurring. However, the accumulation positions of energy in an underground space are still unclear and knowledge about rock bursts cannot be gained from the perspective of energy accumulation. This study analyzed energy accumulation in the strata vertically and found that non-competent strata are the primary carriers of energy accumulation in the interbedding strata. It should be noted that the energy accumulation patterns in the horizontal direction still need further investigation. Based on the energy accumulation rules of both the vertical and horizontal directions, the energy accumulation regions in the surrounding rocks can be ascertained accurately, which can provide a useful reference for the prevention of rock bursts. This study investigated the occurrence mechanism of rock bursts from the perspective of the key energy accumulation strata for the first time, thereby expanding the energy theory of rock bursts and deepening our knowledge of rock burst mechanisms. This should contribute to the prevention of rock bursts from the perspective of energy and enhance the success rates of prevention and management techniques.

6. CONCLUSIONS

This paper used mainly experimental research and theoretical analysis methods, based on energy theory, and has innovated from three aspects. First, unlike previous combinations, a new type of coal-rock combination was established, and new reliable experimental data was obtained. Second, the problem of energy distribution in a coal-rock combination has been studied for the first time. The proportion of the energy of each component before the destruction of the coal-rock combination was obtained through experiments, and the law of energy accumulation was further assessed. Third, on the basis of the above research results, the concept of “key energy strata” was put forward for the first time. From the perspective of energy accumulation, the findings are of great significance with regard to the prevention and control of rock bursts. The specific research results are as follows:

1. Three standard specimens (φ=50mm, h=100mm) of coal, gritstone and fine sandstone were tested under axial loading. It was found that the failure form of coal is in a clastic state, and the fine sandstone has some obvious characteristics of brittle failure. The stress-strain curves of coal specimens have an obvious compaction phase and plastic phase, whilst the elastic phase of gritstone and fine sandstone specimens is more obvious. The uniaxial compressive strength of fine sandstone is the largest, and the uniaxial compressive strength of coal is the smallest. The rule of accumulated energy in front of the peak of three kinds of specimens from more to less is: fine sandstone, gritstone and coal.
2. The composite specimen of coal and rock was constructed and tested under axial loading. The results show that the compressive strength of the composite specimen is almost equal to the compressive strength of the failure component. The smaller the compressive strength of the combined specimen, the smaller the accumulated energy of the combined specimen. Moreover, the larger the difference in the component hardness, the larger the impact energy index, and the stronger the rock burst tendency. In the process of coal seam mining, the harder the roof and floor, the higher the rock burst tendency.
3. The mechanical models of the binary composite specimen and ternary composite specimen were constructed and analyzed. The energy stored in each component of the combined specimen can be calculated and the energy distribution law before the failure of the combined specimen can be obtained. The term "key energy strata" is put forward from the point of view of the energy accumulated horizon, which expands the energy theory of the rock burst, deepens the understanding of the rock burst mechanism, and provides some new thinking for preventing and controlling rock bursts.
4. Through the analysis of the mechanical model, for the coal-bearing binary composite specimens, most of the energy accumulates in the coal component. Furthermore, for the binary specimens composed of fine sandstone and gritstone, most of the energy accumulates in the gritstone component. Finally, for the ternary composite specimens, the coal component accumulates the most energy, and the fine sandstone accumulates the least energy. It can be found that the law of energy distribution of the composite specimens is contrary to that of the standard specimen of coal and rock; the ability to accumulate energy for a competent rock strata with a high elastic moduli is weak, and the energy is accumulated mainly in the non-competent rock strata with a small elastic moduli. Therefore, the non-competent rock strata is the key energy strata.
5. The overlying strata are composed of various rock layers of a different hardness, and the accumulated energy is affected by factors such as

the thickness and mechanical properties of the rock layers. Therefore, the key energy strata is not only a type of non-compentent rock strata, but also a strata-zone made up of several types of non-compentent rock strata.

DATA AVAILABILITY STATEMENT

The authors declare that all data supporting the findings of this study are available within the article, the reader can find and use this data, and there is no unavailable data.

CONFLICTS OF INTEREST

The authors declare that there are no conflicts of interests regarding the publication of this paper.

ACKNOWLEDGMENTS

This research was supported by the National Natural Science Foundation of China (No.51379119，No.51604164).

REFERENCES

Chen, W., Lu, S.P., Guo, X. and Qiao, C.: 2009, Research on unloading confining pressure tests and rock burst criterion based on energy theory. Chinese Journal of Rock Mechanics and Engineering, 28, No. 8, 1530–1540. DOI: 10.3321/j.issn:1000-6915.2009.08.003

Dou, L.M., Lu, C.P., Mou, Z.L., Qin, Y.H. and Yao, J.: 2005, Intensity weakening theory for rock burst and its application. Journal of China Coal Society, 30, No. 6, 690–694. DOI: 10.3321/j.issn:0253-9993.2005.06.003

Dou, L.M., Tian, J.C. and Lu, C.P.: 2005, Research on electro-magnetic radiation rules of composed coal-rock burst failure. Chinese Journal of Rock Mechanics and Engineering, 24, No. 19, 3541–3544.

Fujii, Y., Ishijima, Y., and Deguchi, G.: 1997, Prediction of coal face rock bursts and microseismicity in deep longwall coal mining. International Journal of Rock Mechanics and Mining Sciences, 34, No. 1, 85–96. DOI: 10.1016/S1365-1609(97)80035-4

Gong, W., Peng, Y., Wang, H., He, M., Sousa, L.R.E. and Wang, J.: 2015, Fracture angle analysis of rock burst faulting planes based on true-triaxial experiment. Rock Mechanics and Rock Engineering, 48, No. 3, 1017–1039. DOI: 10.1007/s00603-014-0639-0

Guo, D.M., Zuo, J.P., Zhang, Y. and Yang, R.S.: 2011, Research on strength and failure mechanism of deep coal-rock combination bodies of different inclined angles. Rock and Soil Mechanics, 32, No. 5, 1333–1339. DOI: 10.3969/j.issn.1000-7598.2011.05.009

He, J., Dou, L.M. and Mou, Z.L.: 2016, Numerical simulation study on hard-thick roof inducing rock burst in coal mine. Journal of Central South University, 23, No. 9, 2314–2320. DOI: 10.1007/s11771-016-3289-4

Heriawan, M.N. and Koike, K.: 2008, Identifying spatial heterogeneity of coal resource quality in a multilayer coal deposit by multivariate geostatistics. International Journal of Coal Geology, 73, No. 3-4, 307–330. DOI: 10.1016/j.coal.2007.07.005

Ikari, M.J., Niemeijer, A.R. and Marone, C.: 2015, Experimental investigation of incipient shear failure in foliated rock. Journal of Structural Geology, 77, No. 8, 82–91. DOI: 10.1016/j.jsg.2015.05.012

Kong, X., Wang, E., Hu, S., Shen, R., Li, X. and Zhan, T.: 2016, Fractal characteristics and acoustic emission of coal containing methane in triaxial compression failure. Journal of Applied Geophysics, 124, No. 1, 139–147. DOI: 10.1016/j.jappgeo.2015.11.018

Li, D., Sun, Z., Xie, T., Li, X. and Ranjith, P.G.: 2017, Energy evolution characteristics of hard rock during triaxial failure with different loading and unloading paths. Engineering Geology, 228, No. 10, 270–281. DOI: 10.1016/j.enggeo.2017.08.006

Li, D.Y., Sun, Z., Li, X.B. and Xie, T.: 2016, Mechanical response and failure characteristics of granite under different stress paths in triaxial loading and unloading conditions. Chinese Journal of Rock Mechanics and Engineering, 35, No.2, 3449–3457. DOI: 10.13722/j.cnki.jrme.2016.0815

Li, L.J., Cao, P. and Chen, Y.: 2008, Study on rock burst mechanism and prediction methods in deep mining. Journal of University of South China, 28, No. 4, 23–37.

Liu, D., Yao, Y., Tang, D., Tang, S., Che, Y. and Huang, W.: 2009, Coal reservoir characteristics and coalbed methane resource assessment in huainan and huaibei coalfields. International Journal of Coal Geology, 79, No. 3, 97–112. DOI: 10.1016/j.coal.2009.05.001

Liu, J.X., Tang, C.A. and Zhu, W.C.: 2004, Rock-coal model for studying the rockburst. Chinese Jounal of Geotechnical Engineering, 26, No. 2, 276–280.

Liu, X., Dai, F., Zhang, R. and Liu, J.: 2015, Static and dynamic uniaxial compression tests on coal rock considering the bedding directivity. Environmental Earth Sciences, 73, No. 10, 5933–5949. DOI: 10.1007/s12665-015-4106-3

Liu, Y., Miao, S., Wei, X., Cui, G. and Wang, H.: 2016, Acoustic emission characteristics and energy mechanism evolution of granite damage under triaxial cyclic loading and unloading. Mining Research and Development, 35, No. 6, 72–80.

Li, X., Du, K., and Li, D.: 2015, True triaxial strength and failure modes of cubic rock specimens with unloading the minor principal stress. Rock Mechanics and Rock Engineering, 48, No. 6, 2185–2196. DOI: 10.1007/s00603-014-0701-y

Lu, C. P., Dou, L. M. and Wu, X. G.: 2007, Experimental research on rules of rockburst tendency evolution and acoustic-electromagnetic effects of compound coal-rock samples. Chinese Journal of Rock Mechanics and Engineering, 26, No. 12, 2549–2555. DOI: 10.3321/j.issn:1000-6915.2007.12.022

Mazaira, A. and Konicek, P.: 2015, Intense rockburst impacts in deep underground construction and their prevention. Canadian Geotechnical Journal, 52, No.10, 1426–1439. DOI: 10.1139/cgj-2014-0359

Mohtarami, E., Jafari, A. and Amini, M.: 2014, Stability analysis of slopes against combined circular-toppling failure. International Journal of Rock Mechanics and Mining Sciences, 67, No. 2, 43–56. DOI: 10.1016/j.ijrmms.2013.12.020

Petukhov, I.M. and Linkov, A.M.: 1979, The theory of post-failure deformations and the problem of stability in rock mechanics. International Journal of Rock Mechanics and Mining Sciences & Geomechanics Abstracts, 16, No. 2, 57–76. DOI: 10.1016/0148-9062(79)91444-X

Qi, Q.X. and Dou, L.M.: 2008, Theory and Technology of Rock Burst. China Mining University Press, Xuzhou, China.

Stacey, T.R.: 2016, Addressing the consequences of dynamic rock failure in underground excavations. Rock Mechanics and Rock Engineering, 49, No. 10, 4091–4101. DOI: 10.1007/s00603-016-0922-3

Tang, Z., Yang, S. and Wu, G.: 2017, Occurrence mechanism and risk assessment of dynamic of coal and rock disasters in the low-temperature oxidation process of a coal-bed methane reservoir. Energy and Fuels, 31, No. 4, 3602–3609. DOI: 10.1021/acs.energyfuels.6b03106

Vakili, A. and Hebblewhite, B.K.: 2010, A new cavability assessment criterion for longwall top coal caving. International Journal of Rock Mechanics & Mining Sciences, 47, No. 8, 1317–1329. DOI: 10.1016/j.ijrmms.2010.08.010

Warwick, P.D., Flores, R.M., Affolter, R.H. and Hatch, J.R.: 2002, The US geological survey's national coal resource assessment: the results. International Journal of Coal Geology, 50, No. 1, 247–274. DOI: 10.1016/S0166-5162(02)00120-9

Xie, H.P., Zhou, H.W., Xue, D.J., Wang, H.W., Zhang, R. and Gao, F.: 2012, Research and consideration on deep coal mining and critical mining depth. Journal of China Coal Society, 37, No.37, 535–542. DOI: 10.1007/s11783-011-0280-z

Xiong, X.: 2014, Study on formation mechanism of rock burst and rating prediction based on artificial neural network in rock mass engineering. Nmr in Biomedicine, 3, No. 2, 59–63. DOI: 10.1002/nbm.1940030203

Zhang, J., Jiang, F., Yang, J., Bai, W. and Zhang, L.: 2017, Rock burst mechanism in soft coal seam within deep coal mines. International Journal of Mining Science and Technology, 27, No. 3, 551–556. DOI: 10.1016/j.ijmst.2017.03.011

Zhang, Z. and Feng, G.: 2015, Experimental investigations on energy evolution characteristics of coal , sandstone and granite during loading process. Journal of China University of Mining and Technology, 44, No. 3, 416–422.

Zhao, T.B., Yin, Y.C., Tan, Y.L., Wei, P. and Zou, J.C.: 2014, Bursting liability of coal research of heterogeneous coal based on particle flow microscopic test. Journal of the China Coal Society, 39, No. 2, 280–285. DOI: 10.13225/j.cnki.jccs.2013.2017

Zhao, X.Y., Jiang, Y.D., Zhu, J. and Sun, G.Z.: 2008, Experimental study on precursory information of deformations of coal-rock composite samples before failure. Chinese Journal of Rock Mechanics and Engineering, 27, No. 2, 339–346. DOI: 10.3321/j.issn:1000-6915.2008.02.016

Zhou, Y., Ji, H., Zhang, Y., Hou, Z. and Xiang, P.: 2017, Analysis on acoustic emission characteristics of monzonitic granite during triaxial loading-unloading process. Chinese Journal of Underground Space and Engineering, 13, No. 2, 314–321.

Zhu, W.C., Li, Z.H., Zhu, L. and Tang, C.A.: 2010, Numerical simulation on rock burst of underground opening triggered by dynamic disturbance. Tunnelling and Underground Space Technology Incorporating Trenchless Technology Research, 25, No. 5, 587–599. DOI: 10.1016/j.tust.2010.04.004

Zuo, J.P., Wang, Z.F., Zhou, H.W., Pei, J.L. and Liu, J.F.: 2013, Failure behavior of a rock-coal-rock combined body with a weak coal interlayer. International Journal of Mining Science and Technology, 23, No. 6, 907–912. DOI: 10.1016/j.ijmst.2013.11.005